Interaction of Hydrogen with Cerium Oxide Surfaces: a Quantum Mechanical Computational Study

Gianpaolo Vicario and Gabriele Balducci*

Department of Chemical Sciences, INSTM-Trieste Research Unit and Center of Excellence for Nanostructured Materials, Universitá degli Studi di Trieste, via L.Giorgieri 1, I-34127 Trieste, Italy

Stefano Fabris, Stefano de Gironcoli, and Stefano Baroni

SISSA and INFM-CNR DEMOCRITOS National Simulation Center, Via Beirut 2-4, I-34014 Trieste, Italy

Received: March 6, 2006; In Final Form: July 31, 2006

The interaction of the (110) and (111) surfaces of ceria (CeO_2) with atomic hydrogen is studied with ab initio calculations based on density functional theory. A Hubbard *U* term added to the standard density functional allows to accurately describe the electronic structure of the two surfaces. The minimum energy configuration for the adsorbed H on each of the two surfaces is obtained. An O−H−O bridge is formed on the (110) surface, whereas an axial tricoordinated OH group results on the (111) surface. For both surfaces, the adsorption of an H atom is accompanied by the reduction of a single Ce ion (which is one of the nearest neighbors of the adsorbed atom) and by a substantial outward protrusion of the O atom(s) directly bound to H. The adsorption of atomic H on the (110) and (111) surfaces is energetically favored by −150.8 and −128.3 kJ/mol, respectively, with respect to free molecular H_2. The calculated frequencies for the OH stretching vibrational mode are 3100 cm^{-1} for the (110) surface and 3627 cm^{-1} for the (111) surface. The latter value is in excellent agreement with experimental data reported in the literature.

Introduction

Cerium dioxide (CeO_2, ceria) and related materials show interesting properties that make them technologically attractive. They are currently being used as important components of the "three-way" catalysts, which convert the main pollutants present in vehicle emissions (carbon monoxide, nitric oxides, and unburned hydrocarbons) into harmless compounds[1]. More recently, these materials have attracted great interest in the field of the solid-oxide fuel cells as alternative electrolytes capable of lowering the temperature of operation.[2−4] In the related field of "onboard" hydrogen production via steam reforming of hydrocarbons, ceria-based catalysts are being currently considered as strong candidates for the low-temperature water gas shift reaction, which converts CO and water to CO_2 and hydrogen. Most of these technological applications rely upon the distinctive feature of the Ce ions to easily switch oxidation number between +4 and +3.

Cerium reduction in cerium oxide is known to be triggered by high-temperature treatment under vacuum; however, the same effect can be obtained at lower temperatures when the material is exposed to a chemically reducing atmosphere. This may or may not be an advantage, depending on the particular application. For instance, in solid oxide fuel cells, cerium reduction due to the fuel-rich environment of the anodic compartment increases an undesired electronic conductivity of the material, which significantly degrades its efficiency as solid electrolyte.[5] On the other hand, the ability of cerium oxide to easily react with molecular hydrogen is the basis for its possible use as a hydrogen scavenger in dehydrogenation catalysis.[6] When used as water gas shift reaction catalysts, ceria-based materials operate in a highly reducing environment (hydrogen stream from the reformed hydrocarbons) whose effects on the catalyst and the reaction mechanism are still a topic of debate.[7]

In view of the possibility to tailor the oxido-reductive properties of cerium oxide based materials for a particular application, understanding the factors that govern their interaction with reducing agents is of paramount interest.

Hydrogen has been used as the reducing agent in the majority of the experimental studies on the reduction of ceria.[8−10] Indeed, cerium oxide comes in contact with a hydrogen-containing atmosphere in many practical applications.

For this reason, extensive work has been done in the attempt to clarify the most fundamental aspects of the interaction between cerium dioxide and hydrogen.[11−15]

In this paper, we study the interaction of the (110) and (111) surfaces of ceria with atomic hydrogen by means of ab initio calculations. Important and still unclear issues such as the most stable configuration of adsorbed hydrogen and the details of the electronic structure of the adsorbates will be addressed.

Computational Methods

All the calculations herein presented were performed in the frame of the density functional theory (DFT) with the Quantum-ESPRESSO suite of codes.[16] The crystalline orbitals were expanded in a set of plane waves limited by a kinetic energy cutoff of 40 Ry (determined after an appropriate convergence study). The effect of atomic nuclei together with the inner-core electrons was simulated with ultrasoft pseudopotentials[17] and only valence electrons ($2s^2 2p^4$ for O and $5s^2 5p^6 6s^2 4f^2$ for Ce) were explicitly considered.

Because the only oxidation states visited by the cerium ion in the systems of interest here are +3 and +4, to improve the

* Corresponding author. E-mail: balducci@units.it. Telephone: I-(0)-40-5583957. Fax: I-(0)40-5583903.

10.1021/jp061375v CCC: $33.50
Published on Web 09/14/2006

transferability properties of the cerium pseudopotential, a reference configuration corresponding to an isolated $Ce^{3.5+}$ ion was used for the pseudopotential generation. All technical details regarding the pseudopotentials used in the present study are available upon request from the authors.

The (spin-polarized) generalized gradient approximation (GGA) with the Perdew−Burke−Ernzerhof (PBE) parametrization[18] was used for the exchange-correlation part of the energy functional.

Reciprocal space integrations over the first Brillouin zone (BZ) were approximated by sampling the quantities to be evaluated on a discrete *k*-point grid constructed according to the scheme of Monkhorst and Pack.[19] Proper convergence of the results upon the number of *k*-points was checked for each simulated system.

The DFT + *U* Methodology. The application of "standard" DFT methods to the simulation of cerium oxide based materials poses a special problem due to the multiple valency of the Ce atoms resulting from the different occupancy of the Ce 4f states, which undermines the predictive power of standard DFT calculations. This is evident for the case of cerium sesquioxide, Ce_2O_3, in which one of the 4f states is occupied therefore determining the +3 valency of the Ce ions. Most of the DFT calculations reported so far do not capture the physical insulating ground state but predict a metallic solution.[20] The addition of a Hubbard *U* term to the energy functional (DFT + *U*) has been shown to overcome this problem,[21−26] thus allowing to properly account for the multiple valency of Ce in ceria-based materials.

We have implemented a simplified version of the so-called DFT + *U* method, initially developed by Anisimov and co-workers[27] and further improved by Pickett and co-workers.[28] In essence, the method modifies the standard DFT energy functional according to:

$$E_{\mathrm{DFT}+U} = E_{\mathrm{DFT}} + \frac{U}{2}\sum_{I} Tr(\mathbf{n}^I(1-\mathbf{n}^I)) \qquad (1)$$

where E_{DFT} is the standard DFT (LDA or GGA) functional, and the second term on the right introduces the on-site Coulomb correlation. This latter is made to act only on the 4f orbitals of the Ce atoms. Accordingly, the $\mathbf{n}^I$ terms above are 14×14 occupation matrixes (*I* is the index for the cerium crystal site), obtained by projection of the electron density over suitably chosen localized atomic orbitals, which, in our implementation of the method, were localized Wannier functions[29] obtained from the Ce 4f bands with a subspace alignment procedure.[23,30] Because occupations are bound in the interval [0,1] by taking the first derivative of eq 1 with respect to the occupations, it is seen that scantily occupied states will be destabilized, while heavily occupied ones will feel a stabilizing potential, the effect being scaled by the parameter *U*. The final result is the creation of a gap in the otherwise unsplitted narrow band due to the 4f orbitals of the Ce atoms.

The value $U = 4$ eV was used in our calculations, which gives very good agreement with measured structural and electronic properties of ceria (vide infra). A completely ab initio procedure for the evaluation of *U*, applied after this study was completed, gave a very similar value of $U = 4.5$ eV.[31] In this regard, it must also be added that the use of Wannier functions as projectors for the electron density in order to obtain the **n** matrixes in eq 1 makes the energetics independent of the particular *U* value (as long as *U* is large enough to open a gap in the 4f orbitals of cerium).[31]

Periodic Supercells. Calculations were performed for the (111) and (110) surfaces of ceria with the periodic slab method. The simulated slabs were separated by an empty space of 10 Å, which was found adequate to avoid spurious interactions between facing surfaces of successive slabs along the normal direction.[30] On the basis of appropriate convergence tests, it was found that 6 and 9 atomic layers, for the (110) and (111) surfaces, respectively, were enough to ensure the absence of interactions between opposite faces of the same slab (the accuracy on the surface energy for the (110) and (111) surfaces was 0.001 and 0.002 J/m^2, respectively).

Hydrogen adsorption was simulated at a fixed coverage of 0.5 monolayers with (1×1) and $(1 \times \sqrt{3})$ supercells for the (110) and (111) surfaces, respectively. The coverage is referred to the exposed oxygen atoms of each surface, 0.5 meaning that the number of adsorbed hydrogen atoms is half the number of exposed oxygen atoms.

Vibrational Properties. The OH stretching frequencies were estimated in two steps. First, the classical harmonic vibrational problem was considered:

$$\mathbf{Hu} = \omega^2\,\mathbf{Mu} \qquad (2)$$

where **H** ($H_{ij} = \partial^2 E/\partial u_i \partial u_j$) is the Hessian matrix (*E* is the electronic energy), **u** is the dispacement pattern corresponding to the vibrational mode with angular frequency ω, and **M** is the diagonal matrix of the ionic masses. Because the OH stretching mode has the highest eigenvalue in the vibrational spectrum and is dominated by the displacements of the bonded O and H atoms, an approximation to the associated eigenvector was obtained by displacing the O and H atoms from their relaxed (equilibrium) positions along the O−H direction. This first guess, together with the corresponding vibrational frequency, were then refined iteratively with a Davidson algorithm.[32] The matrix elements needed at each iteration, $\langle \mathbf{u}_k|\mathbf{H}|\mathbf{u}_l\rangle$ ($\mathbf{u}_k$ is the *k*th base element in the orthogonal expansion of the sought eigenvector), were computed as $-\langle \mathbf{u}_k|\Delta\mathbf{f}_l\rangle$ where $\Delta\mathbf{f}_l$ is the vector of the linear variation of the forces acting on each atom of the unit (super)cell calculated from self-consistent electronic energy minimizations with the atoms displaced according to the pattern $\mathbf{u}_l$. At each step of the Davidson procedure, the highest eigenvalue and corresponding eigenvector were taken.

After satisfactory convergence of this first estimation step, a higher-level refinement was implemented in order to take into account both quantum and anharmonicity effects. A Morse potential function was fitted to a series of energy vs amplitude data for the vibrational mode already determined, and the available analytical results for a quantum Morse oscillator could thus be applied.[33]

Results

The (110) is a type I surface[34] consisting of a sequence of stoichiometric CeO_2 atomic layers; the (111) is a type II surface, whose repetition unit along the normal direction is a stack of three atomic O/Ce/O layers.

Before undertaking the study of the interaction with hydrogen, we performed preliminary calculations on the clean surfaces to validate our methodology.[30] The obtained results are in good agreement with currently available data. For example, our relaxed surface energies for the clean (110) and (111) surfaces are 1.06 and 0.72 J/m^2, respectively. These surface energies closely match recently published results.[22,35,36] A similar agreement is obtained for the relaxed slab geometries in both cases.

To test the ability of our methodological setup to quantitatively account for the energetics associated with the valence changes of the cerium atom, we have also evaluated the

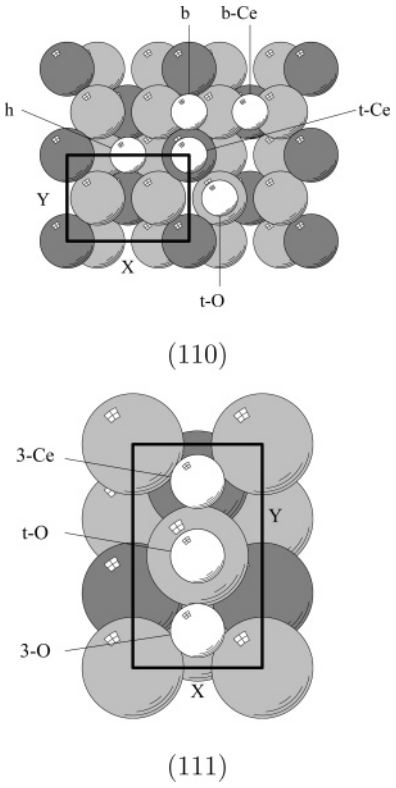

Figure 1. Top view of the (110) and (111) slabs showing the different initial positions of the H atom from which full relaxations were started. Dark-gray, light-gray, and white spheres represent Ce, O, and H atoms, respectively. The surface unit cells and axes for each slab are also shown. The nomenclature of the high-symmetry surface sites for the initial adsorption of H is the following: **h**, hollow site; **b**, bridge with no atoms underneath; **b-Ce**, bridge with a Ce atom underneath; **t-O**, on top of an O atom; **t-Ce**, on top of a Ce atom; **3-O**, 3-fold site with an O atom underneath; **3-Ce**, 3-fold site with a Ce atom underneath.

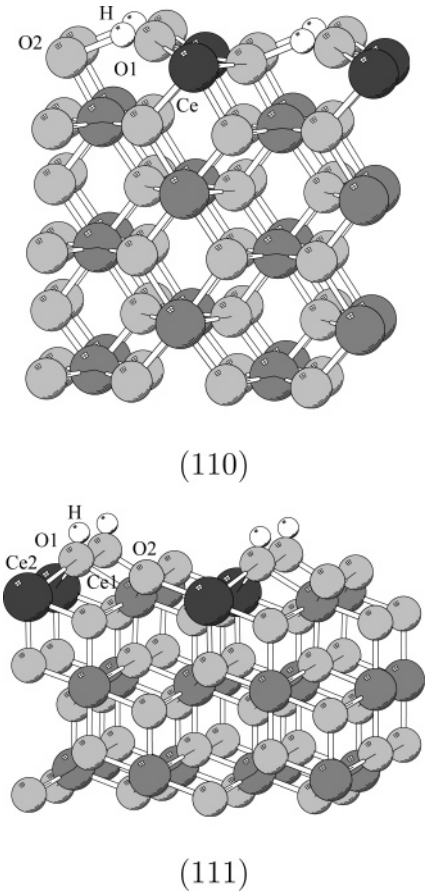

Figure 2. Side view of the relaxed (110) and (111) slabs showing the final position of the adsorbed H atom (white spheres). For the sake of convenience, (2×2) surface cells have been plotted. Atom gray shades as for Figure 1 except for heavy-gray spheres, which represent reduced Ce atoms. Labeled atoms help the reader to identify the fragments reproduced in Figures 3 and 4.

reduction energy of ceria:

$$CeO_2 = \frac{1}{2} Ce_2O_3 + \frac{1}{4} O_2 \qquad (3)$$

The calculated result of 2.28 eV is in satisfactory agreement with the experimental value of 1.98 eV.[37]

A detailed DFT + U study of pure and defective surfaces of ceria with our methodology has been recently published.[30]

To determine the minimum energy configurations of the adsorbed hydrogen, we have performed full structural relaxations of the slabs on which an H atom had been positioned on the different initial sites indicated in Figure 1. The most stable equilibrium configurations are shown in Figure 2.

In the (110) surface, the adsorbed H atom bridges two O atoms (O−H distances: 0.99 Å and 1.85 Å). Of the two possible bridging positions **b** and **b-Ce** (Figure 1), the latter is energetically favored by 1.42 eV.

In the case of the (111) surface, the final, minimum-energy position of the H is on top of an exposed O atom (O−H distance: 0.97 Å). The internuclear O−H direction is almost perpendicular to the surface (the angle between the O−H direction and the surface normal is 6°). A local minimum (1.63 eV higher than the most stable configuration) is obtained when the H atom is placed exactly in the center of a 3-fold site with an underlying O atom (site **3-O** in Figure 1): in this case, the H atom sinks along the normal to the surface up to a distance of 0.99 Å from the O atom of the third atomic layer. However, if the initial H position is slightly moved in order to break the local symmetry, the global minimum is readily recovered. Local symmetry is also responsible for the repulsion observed when the H atom is placed in the **3-Ce** site at the initial Ce−H distance of 0.9 Å). In this case, the H atom relaxes away from the surface along the normal. Similarly to what was observed for the starting position **3-O**, breaking the 3-fold symmetry drives the relaxation of the H atom toward the global minimum, site **t-O**.

The most important geometrical changes (with respect to the relaxed clean surfaces) induced by H adsorption in both cases involve the O atom(s) directly bonded to H and the nearest cerium ions.

In the case of the (110) surface, both the H-bridged O atoms relax toward the H atom: the one closer to H protrudes out of the surface by 0.58 Å, while the other one moves almost exclusively along the direction of the X axis by 0.33 Å. On the opposite, both the surface and subsurface cerium ions move by 0.25 and 0.14 Å, respectively, away from the H atom; the reduced cerium ion (see below) raises above the surface by 0.15 Å. The relaxation of the remaining ions in the supercell is far less significant. As a consequence of these ionic displacements, the Ce−O distances around the surface cerium ion increase with respect to the clean surface by amounts in the range 0.07−0.15 Å.

In the case of the (111) surface, only the oxygen atom directly bonded to H moves significantly, protruding outward by 0.44 Å. The two surface cerium ions move by 0.10 and 0.07 Å only, both away from the H atom and their distances from the

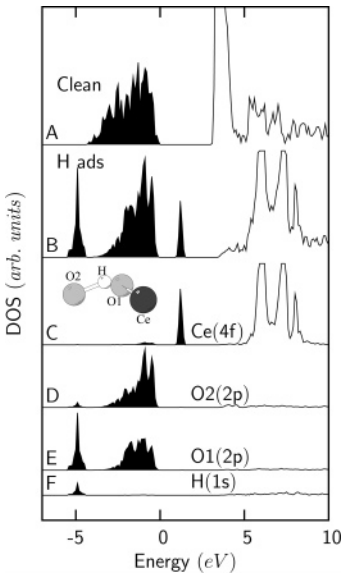

Figure 3. Density of electronic states for the exposed layer of the (110) slab. A: clean (relaxed) surface; B: H-adsorbed surface; C, D, E, F: projection onto selected atomic states (as detailed in the figure) for the atoms of the fragment taken from Figure 2 and reproduced in the inset. The zero of the energy axis has been set at the top of the valence band; occupied states are indicated by shading.

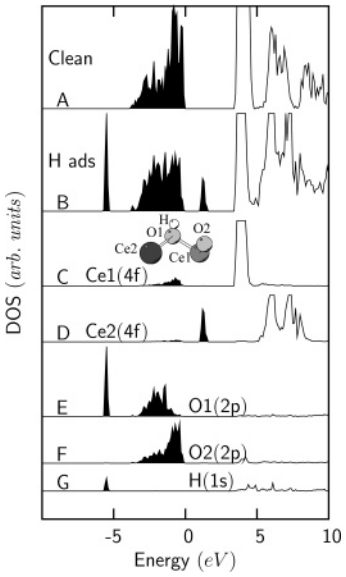

Figure 4. Density of electronic states for the topmost O and Ce layers of the (111) slab. A: clean (relaxed) surface; B: H-adsorbed surface; C, D, E, F, G: projection onto selected atomic states (as detailed in the figure) for the atoms of the fragment taken from Figure 2 and reproduced in the inset. The zero of the energy axis has been set at the top of the valence band; occupied states are indicated by shading.

H-bonded O atom both increase by 0.26 Å (for the reduced cerium ion) and 0.19 Å (for the unreduced cerium ion).

Further details on the adsorption process can be gained by the analysis of the electronic structure in the final relaxed configurations. We find that the adsorption of an H atom yields the reduction of a Ce ion. This is true for both the (111) and (110) surfaces. The reduced Ce ion is always one of the nearest neighbors of the adsorbed hydrogen atom, as shown in Figure 2, where Ce^{3+} ions are evidenced with a darker-gray shade.

The densities of the electronic states (DOS) for the outermost layers and their projection onto the atomic wave functions for the two slabs are shown in Figures 3 and 4. In both cases, H adsorption is accompanied by the appearance of two new peaks in the DOS, at higher and lower energy with respect to the valence band of the clean surface. Projection onto the atomic orbitals of the surface atoms reveals that the peak at higher energy results from the reduction of one Ce ion and, similarly to the Ce_2O_3 bulk phase,[23] is associated with the occupied 4f state of the Ce^{3+} ion. The peak at lower energy results from the hybridization between O 2p and H 1s states.

As one could easily predict from the relaxed geometries, in the case of the (110) surface, both the H-bridged O atoms interact with H, although to a different extent (Figure 3, graphs D, E). On the other hand, in the case of the (111) surface, only one O atom is involved in the bond with H (Figure 4, graphs E, F).

In light of these results, the adsorption process therefore yields the +4/+3 reduction of Ce with the concurrent oxidation of the H atom and the formation of oxy−hydroxy surface species:

$$CeO_2 + H = CeO(OH) \tag{4}$$

The energy change for the above process is −367.4 kJ on the (110) surface and −344.9 kJ on the (111) surface. The corresponding energetics with respect to the H_2 molecule:

$$CeO_2 + \frac{1}{2}H_2 = CeO(OH) \tag{5}$$

are −150.8 and −128.3 kJ, respectively.

With the method described in the previous section, we have calculated the vibration frequency for the stretching of the O−H bond: the values are 3100 and 3627 cm^{-1} for the (110) and (111) surfaces, respectively.

Discussion

The first point to be addressed in the discussion of the obtained results is the DFT + *U* methodology. Recent work[21−24] clearly shows the high predictive power of this method for cerium oxide based materials with respect to current "standard" DFT approaches. Here, it is worth remarking that the use of the DFT + *U* model functional was essential for this study because, as is experimentally well-known, the interaction of hydrogen with ceria leads to its partial reduction and hence to occupation of Ce 4f states. Most of previous computational work on cerium oxides either was focused only on structural properties[38,39] or, when the calculated electronic structure was also analyzed, only the fully oxidized CeO_2 compound was considered.[40,41] The only (to our knowledge) theoretical study specifically dealing with the interaction of hydrogen with bulk ceria did not report any electronic structure results.[42] Recent work,[20,36] however, has clearly evidenced the difficulties that arise when the electronic properties of *partially or fully reduced* cerium oxides are to be calculated and compared with experimental observations due to partial occupation of the Ce 4f bands. Our DFT + *U* implementation overcomes these problems without any a priori assumption.

The calculated density of states for the two surfaces in the presence of adsorbed H are qualitatively similar, the main features being the two new peaks (as compared to the clean surfaces) at higher and lower energy with respect to the O 2p valence band (panels B in Figures 3 and 4). The high-energy peak has been experimentally observed with X-ray and ultraviolet photoelectron spectroscopies for both the (110)[43] and the (111)[44,45] surfaces of partially reduced ceria, and it has been assigned to emission from Ce 4f occupied states. Our calculated electronic structures do capture the essential features of these

experimental observations, confirming the almost exclusive contribution from Ce 4f states to the high-energy peak.

The peak at lower energies with respect to the O 2p valence band has also been experimentally observed for the (111) surface and tentatively attributed to emission from occupied states of OH groups strongly interacting with Ce^{3+} centers.[45] Our calculations confirm this assignment and predict a very similar situation for the (110) surface.

For both surfaces, we find that the adsorbed H atom transfers its electron to a single Ce atom, thus causing its oxidation state to change from +4 to +3. The reduced Ce atom is always one of the nearest neighbors of the adsorbed hydrogen: in the (110) case, it is one of the exposed Ce ions, whereas in the (111) slab, it belongs to the Ce layer immediately under the exposed O atomic layer (Figure 2). Trying to force reduction of an inner Ce ion has no effect in the sense that the Ce^{3+} center is always found in the same position after relaxation. This tendency to segregate at the surface is interpreted mainly in terms of the increase in size of the reduced Ce atoms.

In the case of the (111) supercell, there are two independent cerium ions bonded to the OH group: one is a formal Ce^{3+} species (Ce2 in Figure 4), while the other has a formal valence +4 (Ce1 in Figure 4). As is seen from the projected density of states (Figure 4C), the unreduced cerium ion shows some hybridization of its 4f orbitals with the 2p ones of the oxygen atoms. A comparison with the clean surface (not reported here) shows negligible difference in this hybridization, suggesting that the presence of the OH group and the Ce^{3+} ion do not affect to a noticeable extent the (small) covalency of the Ce^{4+} species.

The final adsorption geometry on the (111) surface (H atom on top of an exposed O atom) has been experimentally observed with noncontact atomic force microscopy as a set of 0.3−0.5 Å high protrusions.[46] This reported height is in good accord with our calculated outward protrusion of the H-bonded O atom (0.44 Å).

The final geometry for the (110) surface gives support to previously postulated H-bonded surface OH groups in polycrystalline CeO_2 samples.[14,47] The higher stability when the bridging H atom is sitting above a Ce ion (compare **b** with **b-Ce** in Figure 1) seems to be explainable more with electrostatic than chemical bonding arguments. In fact, while we do not find any appreciable hybridization between the bridging H and the underlying Ce^{4+} ion, it can be noted that, in the **b** site, the (positively charged) H atom feels an electrostatic repulsion from two nearest-neighbor Ce^{3+} species, while in the **b-Ce** site, only one cation (although of formal charge +4) is at a nearest-neighbor distance.

From an experimental point of view, the interaction of hydrogen with ceria is generally interpreted in terms of irreversible or reversible reduction, according to whether water evolution (and hence O vacancy formation) is or is not observed, respectively, upon hydrogen treatment.[48] Our calculations provide a sensible description of the hydrogen adsorption process and of its final minimum energy configuration, which unambiguously shows concomitant reduction of one Ce ion per adsorbed H atom. Of course, whether this first step is or is not followed by water evolution (irreversible reduction) depends on several experimental conditions such as temperature, partial pressure of the gaseous reactants (H_2, H_2O), and the possible presence of surface modifiers, which could lower the activation energy for H_2 splitting and/or H_2O formation. Our 0 K computational study does not allow any insight about the different possible mechanisms for water desorption, but for the observation that formation of the surface OH groups causes an important protrusion of the H-bonded O atoms and thus the lengthening of the corresponding Ce−O bonds, which might be the starting point for water desorption, under favorable experimental conditions.

On the other hand, our calculations do not support the possible formation of a hydride surface species, which has been suggested in the past in order to explain the changes induced by D_2 treatment in the infrared spectrum of hydroxylated ceria.[11] It cannot be excluded, however, that O vacancies or other types of defects could favor the formation of such a species: the influence of defects on the interaction between ceria and hydrogen will be analyzed in a future work.

The negative values of the calculated energy changes for reaction 5 indicate that the dissociative adsorption of molecular hydrogen is energetically favored at 0 K on both the (110) and the (111) surfaces. This result does not change if zero-point vibrational energies are taken into account because the zero-point energy for molecular hydrogen is 26.1 kJ/(mol of H_2),[49] and from our analysis of the OH vibration frequencies, it can be estimated that the zero-point energy of the H-adsorbed systems is of the order of 20 kJ/(mol of H). Although we are not aware of any experimental determination of the adsorption energy of hydrogen on ceria, the value of −43.4 kJ/(mol of H) calculated for inclusion of an hydrogen atom in the bulk[42] seems to be in line with our results.

The reduction of ceria by molecular hydrogen has been extensively studied with infrared spectroscopy.[11,14,50] Mono-, bi-, and tricoordinate surface OH groups have been identified with characteristic IR frequencies at 3710, 3660, and 3600 cm^{-1}, respectively. The minimum energy configuration found for the H atom on the (111) surface corresponds to a tricoordinate OH group, and our calculated stretching frequency of 3627 cm^{-1} is in very good agreement with the experimental results.

The comparison for the case of the (110) surface is less satisfactory, as our computed value of 3100 cm^{-1} is lower than values in the range 3400−3450 cm^{-1} reported in the literature for H-bonded OH groups in ceria.[11,14,47,50]

A possible explanation for this disagreement is that all experimental measurements are performed on polycrystalline samples at high temperatures, most often with a number of annealing cycles, which may reduce the fraction of exposed (110) surface.

Another factor which might affect the calculated vibrational frequency is H coverage. While we only considered here a coverage of 0.5 monolayers (referred to the total available adsorption sites) and did not attempt to study the dependence of the OH stretching vibration on the surface coverage, it is likely that coverage effects are more important for the (110) surface due to the obtained O−H−O bridge configuration. In this regard, it is worth remarking that, in all the available experimental studies on polycrystalline samples, the surface coverage is not quoted.

A third aspect to be considered with respect to the calculated OH frequency for the (110) surface is the nature of the adsorbed hydrogen atom. The correct treatment of the H bond is intrinsically difficult, and small inaccuracies in its representation may cause large errors in the bond strength. As a matter of fact, a previous attempt using the local density approximation (LDA) gave us a value of 2880 cm^{-1}; the limitations of LDA in describing the H bond are well-known, and the use of GGA clearly improves our estimation. However, this trend suggests that the PBE functional might still contain some inadequacies. In this regard, it is worth noting that, for the case of the (111) surface, in which no H bond is present, the LDA value found

for the OH stretching frequency is 3611 cm^{-1}, closely matching the GGA result.

Conclusions

In this paper we have used ab initio computational methods to study the interaction of atomic hydrogen with the (110) and (111) surfaces of CeO_2.

For both surfaces, starting from a number of different initial configurations for the adsorbed H atom, we find that a single final configuration is reached upon relaxation: the H atom bridges two surface O atoms in the (110) surface, while it sticks on top of an O atom in the case of the (111) surface.

The use of a DFT + U methodology allows calculation of electronic structures in good agreement with experimental results. From the analysis of the projected density of states, it can be seen that the adsorption of an H atom causes the +4/+3 reduction of a single Ce ion, which is always one of the nearest neighbors of the adsorbed hydrogen. Whether this first step is or is not followed by water desorption depends on several experimental conditions, whose proper simulation is beyond the scope of the present study.

Adsorption energies for the (110) and (111) surfaces are −150.8 and −128.3 kJ/mol, respectively, indicating that the adsorption of molecular hydrogen on these surfaces of ceria is energetically favored.

The OH stretching frequencies in the final relaxed configurations of the two surfaces were estimated. The one for the (111) surface, 3627 cm^{-1}, is in very close agreement with the experimental value reported for a tricoordinated OH group; the value of 3100 cm^{-1} calculated for the (110) surface is considerably lower than the values quoted in the literature for an H-bonded OH group. Reasons for this disagreement might be the low population of (110) exposed facets in the polycrystalline samples used in the experiments, a possible dependence of the stretching frequency upon the coverage and/or the partial inadequacy of the exchange-correlation functional used in the calculations.

Acknowledgment. Calculations have been made possible by the SISSA−CINECA scientific agreement and by the allocation of computer resources from INFM Progetto Calcolo Parallelo. University of Trieste and Centre of Excellence for Nanostructured Materials, INSTM, FISR2002 "Nanosistemi inorganici ed ibridi per lo sviluppo e l'innovazione di celle a combustibile", FIRB2001 contract no. RBNE0155X7, are gratefully acknowledged for financial support.

Note Added after ASAP Publication. This paper was published ASAP on September 14, 2006. Adsorption energies for (110) and (111) were changed. The updated paper was reposted on September 19, 2006.

References and Notes

(1) Shelef, M.; Graham, G. W.; McCabe, R. W. Ceria and Other Oxygen Storage Components in Automotive Catalysts. In *Catalysis by Ceria and Related Materials*; Trovarelli, A., Ed.; Imperial College Press: London, 2002; Vol. 2.

(2) Hibino, T.; Hashimoto, A.; Inoue, T.; Tokuno, J.; Yoshida, S.; Sano, M. *Science* **2000**, *288*, 2031.

(3) Mogensen, M.; Sammes, N. M.; Tompsett, G. A. *Solid State Ionics* **2000**, *129*, 63.

(4) Park, S. D.; Vohs, J. M.; Gorte, R. J. *Nature* **2000**, *404*, 265.

(5) Steele, B.; Heinzel, A. *Nature* **2001**, *414*, 345.

(6) de Graaf, E. A.; Andreini, A.; Hensen, E. J. M.; Bliek, A. *Appl. Catal., A* **2004**, *262*, 201.

(7) Jacobs, G.; Patterson, P. M.; Williams, L.; Chenu, E.; Sparks, D.; Thomas, G.; Davis, B. H. *Appl. Catal., A* **2004**, *262*, 177.

(8) Binet, C.; Badri, A.; Lavalley, J. C. *J. Phys. Chem.* **1994**, *98*, 6392.

(9) El Fallah, J.; Boujana, S.; Dexpert, H.; Kiennemann, A.; Majerus, J.; Touret, O.; Villain, F.; Le Normand, F. *J. Phys. Chem.* **1994**, *98*, 5522.

(10) Lyons, D. M.; McGrath, J. P.; Morris, M. A. *J. Phys. Chem. B* **2003**, *107*, 4607.

(11) Badri, A.; Binet, C.; Lavalley, J. C. *J. Chem. Soc., Faraday Trans.* **1996**, *92*, 4669.

(12) Bernal, S.; Calvino, J. J.; Cifredo, G. A.; Rodriguez Izquierdo, J. M. *J. Phys. Chem.* **1995**, *99*, 11794.

(13) Bernal, S.; Calvino, J. J.; Cifredo, G. A.; Gatica, J. M.; Omil, J. A. P.; Pintado, J. M. *J. Chem. Soc., Faraday Trans.* **1993**, *89*, 3499.

(14) Laachir, A.; Perrichon, V.; Badri, A.; Lamotte, J.; Catherine, E.; Lavalley, J. C.; Elfallah, J.; Hilaire, L.; Lenormand, F.; Quemere, E.; Sauvion, G. N.; Touret, O. *J. Chem. Soc., Faraday Trans.* **1991**, *87*, 1601.

(15) Fierro, J. L. G.; Soria, J.; Sanz, J.; Rojo, J. M. *J. Solid State Chem.* **1987**, *66*, 154.

(16) Baroni, S.; Dal Corso, A.; de Gironcoli, S.; Giannozzi, P.; Cavazzoni, C.; Ballabio, G.; Scandolo, S.; Chiarotti, G.; Focher, P.; Pasquarello, A.; Laasonen, K.; Trave, A.; Car, R.; Marzari, N.; Kokalj, A. *Quantum-ESPRESSO*; http://www.quantum-espresso.org.

(17) Vanderbilt, D. *Phys. Rev. B* **1990**, *41*, 7892.

(18) Perdew, J. P.; Burke, K.; Ernzerhof, M. *Phys. Rev. Lett.* **1996**, *77*, 3865.

(19) Monkhorst, H. J.; Pack, J. P. *Phys. Rev. B* **1976**, *13*, 5188.

(20) Skorodumova, N. V.; Ahuja, R.; Simak, S. I.; Abrikosov, I. A.; Johansson, B.; Lundqvist, B. I. *Phys. Rev. B* **2001**, *64*, 115108.

(21) Jiang, Y.; Adams, J. B.; van Schilfgaarde, M. *J. Chem. Phys.* **2005**, *123*, 064701.

(22) Nolan, M.; Grigoleit, S.; Sayle, D. C.; Parker, S. C.; Watson, G. W. *Surf. Sci.* **2005**, *576*, 217.

(23) Fabris, S.; de Gironcoli, S.; Baroni, S.; Vicario, G.; Balducci, G. *Phys. Rev. B* **2005**, *71*, 041102(R).

(24) Nolan, M.; Parker, S. C.; Watson, G. W. *Surf. Sci.* **2005**, *595*, 223.

(25) Nolan, M.; Parker, S. C.; Watson, G. W. *J. Phys. Chem. B* **2006**, *110*, 2256.

(26) Nolan, M.; Parker, S. C.; Watson, G. W. *Phys. Chem. Chem. Phys.* **2006**, *8*, 216.

(27) Anisimov, V. I.; Zaanen, J.; Andersen, O. K. *Phys. Rev. B* **1991**, *44*, 943.

(28) Pickett, W. E.; Erwin, S. C.; Ethridge, E. C. *Phys. Rev. B* **1998**, *58*, 1202.

(29) Marzari, N.; Vanderbilt, D. *Phys. Rev. B* **1997**, *56*, 12847.

(30) Fabris, S.; Vicario, G.; Balducci, G.; de Gironcoli, S.; Baroni, S. *J. Phys. Chem. B* **2005**, *109*, 22860.

(31) Fabris, S.; de Gironcoli, S.; Baroni, S.; Vicario, G.; Balducci, G. *Phys. Rev. B* **2005**, *72*, 237102.

(32) Davidson, E. R. *J. Comput. Phys.* **1975**, *17*, 817.

(33) Matsumoto, A. *J. Phys. B: At. Mol. Opt. Phys.* **1988**, *21*, 2863.

(34) Tasker, P. W. *J. Phys. C: Solid State Phys.* **1979**, *12*, 4977.

(35) Skorodumova, N. V.; Baudin, M.; Hermansson, K. *Phys. Rev. B* **2004**, *69*, 075401.

(36) Yang, Z. X.; Woo, T. K.; Baudin, M.; Hermansson, K. *J. Chem. Phys.* **2004**, *120*, 7741.

(37) Eyring, L. The Binary Rare Earths Oxides. In *Handbook on the Physics and Chemistry of Rare Earths*; Gschneider, K. A.; Eyring, L., Eds.; North-Holland: Amsterdam, 1979; Vol. 3, Chapter 27.

(38) Pickard, C. J.; Winkler, B.; Chen, R. K.; Payne, M. C.; Lee, M. H.; Lin, J. S.; White, J. A.; Milman, V.; Vanderbilt, D. *Phys. Rev. Lett.* **2000**, *85*, 5122.

(39) Hirosaki, N.; Ogata, S.; Kocer, C. *J. Alloys Compd.* **2003**, *351*, 31.

(40) Hill, S. E.; Catlow, C. R. A. *J. Phys. Chem. Solids* **1993**, *54*, 411.

(41) Gennard, S.; Cora, F.; Catlow, C. R. A. *J. Phys. Chem. B* **1999**, *103*, 10158.

(42) Sohlberg, K.; Pantelides, S. T.; Pennycook, S. J. *J. Am. Chem. Soc.* **2001**, *123*, 6609.

(43) Mullins, D. R.; Overbury, S. H.; Huntley, D. R. *Surf. Sci.* **1998**, *409*, 307.

(44) Henderson, M. A.; Perkins, C. L.; Engelhard, M. H.; Thevuthasan, S.; Peden, C. H. F. *Surf. Sci.* **2003**, *526*, 1.

(45) Pfau, A.; Schierbaum, K. D. *Surf. Sci.* **1994**, *321*, 71.

(46) Namai, Y.; Fukui, K. I.; Iwasawa, Y. *Catal. Today* **2003**, *85*, 79.

(47) Li, C.; Sakata, Y.; Arai, T.; Domen, K.; Maruya, K.; Onishi, T. *J. Chem. Soc., Faraday Trans. 1* **1989**, *85*, 1451.

(48) Boaro, M.; Vicario, M.; Deleitenburg, C.; Dolcetti, G.; Trovarelli, A. *Catal. Today* **2003**, *77*, 407.

(49) Balakrishnan, A.; Smith, V.; Stoicheff, B. P. *Phys. Rev. A* **1994**, *49*, 2460.

(50) Binet, C.; Daturi, M.; Lavalley, J. C. *Catal. Today* **1999**, *50*, 207.